This is a repository copy of *The crystal structure, morphology and mechanical properties of diaquabis(omeprazolate)magnesium dihydrate*.

White Rose Research Online URL for this paper:
http://eprints.whiterose.ac.uk/160279/

Version: Published Version

Article:

The crystal structure, morphology and mechanical properties of diaquabis(omeprazolate)magnesium dihydrate

Hanane Abouhakim,[a] Sten O. Nilsson Lill,[b]* Michael J. Quayle,[c]
Stefan T. Norberg,[c] Ali Hassanpour[a]* and Christopher M. Pask[a]

[a]School of Chemical and Process Engineering, University of Leeds, Leeds LS2 9JT, UK, [b]Early Product Development and Manufacturing, Pharmaceutical Sciences, R and D, AstraZeneca Gothenburg, Pepparedsleden 1, Mölndal SE-431 83, Sweden, and [c]Pharmaceutical Technology and Development, AstraZeneca Gothenburg, Pepparedsleden 1, Mölndal SE-431 83, Sweden. *Correspondence e-mail: sten.nilsson-lill@astrazeneca.com, a.hassanpour@leeds.ac.uk

The crystal structure of diaquabis(omeprazolate)magnesium dihydrate (DABOMD) in the solid state has been determined using single-crystal X-ray diffraction. Single crystals of DABOMD were obtained by slow crystallization in ethanol with water used as an antisolvent. The crystal structure shows a dihydrated salt comprising a magnesium cation coordinating two omeprazolate anions and two water molecules (W1) that are strongly bound to magnesium. In addition, two further water molecules (W2) are more weakly hydrogen-bonded to the pyridine nitrogen atom of each omeprazolate anion. The crystal structure was utilized to estimate key material properties for DABOMD, including crystal habit and mechanical properties, which are required for improved understanding and prediction of the behaviour of particles during pharmaceutical processing such as milling. The results from the material properties calculations indicate that DABOMD exhibits a hexagonal morphology and consists of a flat slip plane through the (100) face. It can be classed as a soft material based on elastic constant calculation and exhibits a two-dimensional hydrogen-bonding framework. Based on the crystal structure, habit and mechanical properties, it is anticipated that DABOMD will experience large disorder accompanied by plastic deformation during milling.

1. Introduction

Omeprazole (IUPAC name: 6-methoxy-2-[(4-methoxy-3,5-dimethyl-2-pyridyl)methylsulfonyl]-1*H*-benzimidazole) is an active pharmaceutical ingredient (API) known as a proton pump inhibitor (PPI) which inhibits gastric acid secretion and its related disorder in mammals (Gustavsson & Kjellbom, 1997; Toplak Casar, 2013). The original drug was developed by AstraZeneca and marketed as Losec as a racemate which encompasses a tri-coordinated sulfur atom in a pyramidal configuration, which provides two optically active enantiomers, (*S*)- and (*R*)-omeprazole (Hultman *et al.*, 2007; Bhatt & Desiraju, 2007; Mishra *et al.*, 2015). The *S*-isomer (esomeprazole) exhibits a higher bioavailability, resulting in higher plasma concentrations compared with the *R*-isomer, and was launched under the brand Nexium in 2001 (Murakami *et al.*, 2009). The API has also been presented in various salt forms as a means of increasing stability (Skieneh *et al.*, 2016). In this work, the studied salt is the racemic form of diaquabis(omeprazolate)magnesium(II) dihydrate (DABOMD).

APIs in the solid form are often milled to achieve a desirable particle size prior to blending and tabletting. To enable a better understanding of the milling behaviour of the bulk
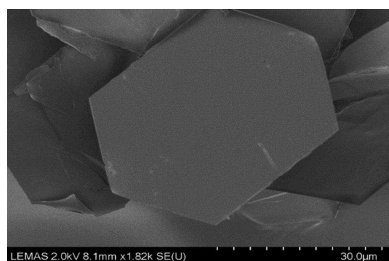
powder, material properties at the single-particle level need to be investigated (Halme *et al.*, 2019; Storey & Ymen, 2011). Obtaining a crystal structure is key to being able to model and simulate the physical and mechanical properties of powders which influence powder-processing properties. However, the crystal structure of DABOMD has not previously been reported to the best of our knowledge. Some literature reports have reported the crystalline structure of omeprazole itself (Ohishi, 1990) and magnesium esomeprazole water–butanol solvate (Skieneh *et al.*, 2016), but no study exists which reports the crystal structure of the parent diaquabis(omeprazolate)magnesium dihydrate (DABOMD).

The crystal structure and its properties greatly influence the formulation and processability of solid dosage forms (Putra *et al.*, 2016). Thus, the aim of this study was first to solve the crystal structure of DABOMD and from that to employ an approach combining experiments and molecular modelling to obtain details of the mechanical property behaviour of DABOMD based on its crystal structure and morphology. A similar modelling approach has previously been applied for various organic pharmaceuticals, *e.g.* aspirin and primidone (Payne, 1996), ibuprofen (Roberts *et al.*, 1994; Beyer *et al.*, 2001) and salbutamol sulfate (Day *et al.*, 2001; Shariare *et al.*, 2012; Halme *et al.*, 2019; Putra *et al.*, 2016).

2. Materials and methods

2.1. Crystallization

Racemic magnesium omeprazole (*R*, *S*) crystalline powder (98% purity) was provided by AstraZeneca. Single crystals of DABOMD (Fig. 1) were obtained by vapour diffusion at room temperature from a saturated solution of DABOMD in ethanol (99% pure) using water as an antisolvent.

2.2. Single-crystal X-ray diffraction

Single-crystal X-ray diffraction (XRD) measurements were conducted at 120 K on an Agilent SuperNova diffractometer equipped with an Atlas CCD detector and connected to an Oxford Cryostream low-temperature device using mirror-monochromated Cu $K\alpha$ radiation (λ = 1.54184 Å) from a Microfocus X-ray source. The DABOMD structure was solved
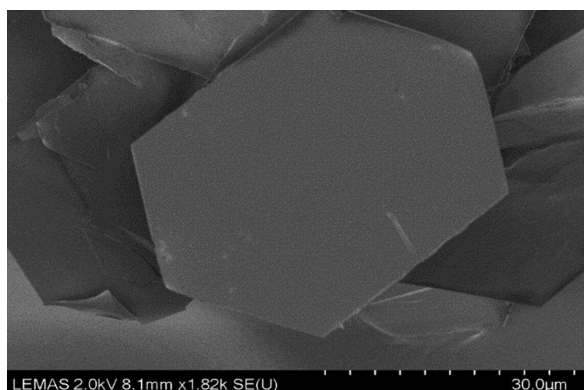
Figure 1
Scanning electron microscopy image of DABOMD single crystals.

using the *SHELXT* intrinsic phasing method (Sheldrick, 2015a) and refined using the *SHELXL2014* full-matrix least-squares technique based on F^2 (Sheldrick, 2015b).

The non-hydrogen atoms were refined anisotropically, whereas the hydrogen atoms were positioned and refined isotropically using a riding model. Anisotropic displacement parameters of the omeprazolate anions were restrained using a rigid-bond restraint. The crystal structure determined under the above conditions has been deposited in the Cambridge Structural Database, refcode 1920020.

2.3. X-ray powder diffraction

X-ray powder diffraction (XRPD) analysis was carried out to confirm that the powder patterns corresponded to the correct structure prior to other bulk analytical techniques. The data were recorded for DABOMD using a Phillips PW 1710 X-ray diffractometer using Cu $K\alpha$ radiation (1.54184 Å) at 40 kV and 30 mA setting. Scans were collected over a 2θ range of 5–55° and an angular step of $2\theta = 0.02°$ using a fixed slit (3°) with 0.25 s per step. The results were compared with a simulated XRPD pattern obtained from the single crystal structure model.

2.4. Thermal analysis

Differential scanning calorimetry (DSC) analysis of the powder of DABOMD was carried out using a Mettler TC 3000 differential scanner calorimeter, with purged liquid nitrogen, at a rate of 5 K min^{-1} from 298 to 563 K. Approximately 5–6 mg of powder was placed in an aluminium sealed pan with a hole on the top. Similarly, thermogravimetric analysis (TGA) was carried out with flowing gaseous nitrogen at a rate of 5 K min^{-1} from 298 to 523 K. A TA Universal Analysis 2000 instrument was used for the analysis.

2.5. Computational approaches

To validate the hydrogen positions in the water molecules of DABOMD, two alternative structures with different hydrogen-bonding patterns were constructed using *Materials Studio* (Dassault Systèmes) starting from the experimental crystal structure. Only the hydrogen positions in the water were altered. These structures were further refined to find the optimal hydrogen bonding, and relative energies were calculated using dispersion-corrected density functional theory. Calculations under periodic boundary conditions were performed using the *Cambridge Serial Total Energy Package* (*CASTEP*, Version 17.1.0.48; Clark *et al.*, 2005). For all tasks (*i.e.* geometry optimizations and energy calculations), the generalized gradient approximation (GGA) density functional theory (DFT) exchange-correlation (XC) functional of Perdew, Burke and Ernzerhof (PBE; Perdew *et al.*, 1996) was used. Core electrons were modelled with ultrasoft pseudopotentials that were generated on the fly. Valence electrons were described using a plane-wave basis with a kinetic energy cutoff of 620 eV. Reciprocal-space sampling of the Brillouin zone used a fixed k-point spacing of 0.05 Å^{-1}. Unit cells were fixed to the experimentally determined cell parameters, and

the dispersion correction of Grimme (D2) was always applied. Self-consistent field (SCF) energy minimizations were performed until a threshold of 1×10^{-6} eV per atom was reached, and geometry optimizations continued until the total energy converged to 1×10^{-5} eV per atom with a maximum ionic force of 3×10^{-2} eV Å^{-1}. Lattice symmetry was used to increase the calculation efficiency.

Mercury (Version 3.9; Macrae *et al.*, 2008) was used to visualize the crystal packing, to analyse the hydrogen bonding and to generate simulated powder X-ray diffraction patterns for DABOMD using the single-crystal structure. Moreover, *Mercury* was also used to model the morphology of DABOMD using the BFDH model (Docherty *et al.*, 1988). The BFDH model is based on the lattice geometry and symmetry and was proposed by Bravais, Friedel, Donnay and Harker. This model assumes that the energetically most stable and slowest growing faces are the ones with the highest density and largest spacing between adjacent layers and that the rate of growth of a particular surface is inversely proportional to the interplanar *d* spacing (Beyer *et al.*, 2001). To quantify the degree of structural agreement between crystal structures, a common method within *Mercury* is to overlay a cluster of 15 molecules from each crystal structure and calculate the root-mean-square distance between heavy atoms (RMSD$_{15}$ value).

The molecular modelling software *Materials Studio* (Dassault Systèmes) was used to calculate the growth morphology and elastic constants of DABOMD. For the growth morphology, the universal force field was employed. Other force fields were tested but were not applicable to magnesium salts. To verify the accuracy of the force field (FF) we made an overlay of the FF-optimized crystal structure with a *CASTEP* optimized structure and found an RMSD$_{15}$ value of 0.4, thus a good agreement. Growth morphology calculations were based on the attachment energy model. The attachment energy, E_{att}, is defined as the energy released on the attachment of a growth slice to a growing crystal face, and is calculated using (Bandyopadhyay & Grant, 2002)

$$E_{att} = E_{lattice} - E_{slice}, \tag{1}$$

where $E_{lattice}$ is the lattice energy of the crystal and E_{slice} is the energy released on the formation of a growth slice of a thickness equal to the interplanar *d* spacing for the crystallographic plane that represents a face attachment. This method is commonly employed to predict crystal morphologies, and is also employed in this work to characterize and identify the crystal planes that are the most weakly interacting and could serve as the slip planes (Sun & Kiang, 2008; Wang & Sun, 2018, 2019).

The mechanical properties, *e.g.* elastic constants (Young's modulus), were calculated using *CASTEP* with settings as described above (Gaillac, 2016).

Crystal Interaction (*CrysIn*), a tool developed in-house, was used to evaluate the static interactions between molecules present in a crystal based on DFT. The intermolecular interaction energies in the first coordination cell of each molecule in the asymmetric unit of the crystal were calculated using B3LYP-D3/6-31G(d,p) as reported in *GAUSSIAN16* (Frisch *et*

Table 1
DABOMD crystal data.

Empirical formula	$C_{34}H_{40}MgN_6O_8S_2 \cdot 2H_2O$
Formula weight	785.18
Temperature (K)	120.0 (2)
Crystal system	Monoclinic
Space group	$P2_1/c$
a (Å)	17.475 (9)
b (Å)	8.051 (2)
c (Å)	14.190 (5)
α (°)	90
β (°)	109.91 (5)
γ (°)	90
Volume (Å^3)	1877.1 (14)
Z	2
ρ_{calc} (g cm^{-3})	1.389
μ (mm^{-1})	1.994
$F(000)$	828.0
Crystal size (mm)	$0.11 \times 0.03 \times 0.01$
Radiation	Cu $K\alpha$ (λ = 1.54184 Å)
2θ range for data collection (°)	10.768 to 147.15
Index ranges	$-15 \leq h \leq 21$
	$-9 \leq k \leq 9$
	$-15 \leq l \leq 17$
Reflections collected	8269
Independent reflections	3546 (R_{int} = 0.1656, R_{sigma} = 0.2009)
Data, restraints, parameters	3546, 216, 249
Goodness of fit on F^2	1.072
Final R indexes [$I \geq 2\sigma(I)$]	R_1 = 0.1496, wR_2 = 0.3519
Final R indexes (all data)	R_1 = 0.2299, wR_2 = 0.4164
Largest difference peak/hole (e Å^{-3})	1.71, −0.66

al., 2016). This is a comparable method to that employed in, for instance, the energy framework calculations in *Crystal-Explorer* (Turner *et al.*, 2015) or *PIXEL* (Gavezzotti, 2005). This approach enables the quantification of the intermolecular interactions present in a crystal and can thus lead to the identification of slip planes with the weakest interactions. The Miller planes in the crystal at which the weakest interactions occur, and the dimer interactions spanning over those Miller planes, can be identified through visualization (Halme *et al.*, 2019).

3. Results and discussion

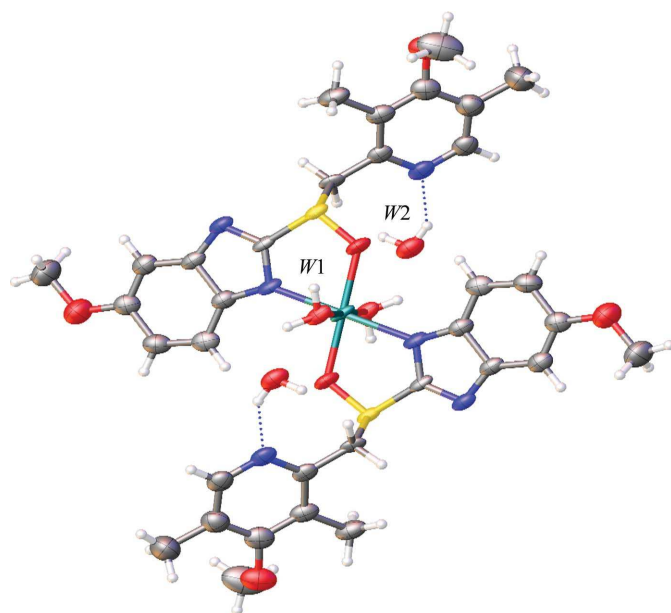### 3.1. Crystal structure of diaquabis(omeprazolate)magnesium dihydrate

Despite being developed in the early 1990s, no single-crystal structure determination has been published for DABOMD. This is potentially due to difficulties in growing single crystals of appropriate quality and size. In this work, the vapour diffusion method yielded hexagonal platelet single crystals with dimensions $0.11 \times 0.03 \times 0.01$ mm after approximately two weeks (Fig. 1).

DABOMD crystallizes in the monoclinic space group $P2_1/c$ [Z = 2, a = 17.475 (9) Å, b = 8.051 (2) Å, c = 14.190 (5) Å; β = 109.91 (5)°]. The crystallographic data are summarized in Table 1, with selected bond lengths and bond angles shown in Tables 2 and 3, respectively. The asymmetric unit consists of one omeprazolate anion, two water molecules and 0.5 magnesium cation. The quality of the refinement is moderate (R_1 = 0.150) caused by the thin platelet crystal. Applying the

Table 2
Selected bond lengths for DABOMD.

Atom	Atom	Length (Å)
Mg1	O1	2.086 (7)
Mg1	O4	2.084 (7)
Mg1	N1	2.168 (8)

Table 3
Selected bond angles for DABOMD.

Atom	Atom	Atom	Angle (°)
O1^i	Mg1	N1	81.3 (3)
O1	Mg1	N1	98.7 (3)
O4^i	Mg1	O1	87.6 (3)
O4^i	Mg1	O1	92.4 (3)
O4	Mg1	N1	87.3 (3)
O4	Mg1	N1	92.7 (3)
S1	O1	Mg1	120.6 (4)
C4	O2	C7	117.9 (11)
C12	O3	C16	115.1 (12)
C1	N1	Mg1	140.6 (6)
C8	N1	Mg1	116.1 (7)
C8	N1	C1	103.3 (8)
C8	N2	C6	103.3 (8)
C10	N3	C14	117.3 (10)
N1	C1	C2	131.9 (10)
N1	C1	C6	107.1 (9)

Symmetry code: (i) $-x, -y, -z$.

symmetry operations of $P2_1/c$ gives DABOMD with two anions of omeprazolate and two molecules of water ($W1$), positioned around a twofold axis, coordinated to one central magnesium cation which occupies an inversion centre (Fig. 2). The magnesium shows a distorted octahedral geometry, with *cis* bond angles around the magnesium ranging from 81.3 (3) to 98.7 (3)°. Mg—O and Mg—N bond lengths of 2.086 (7) and 2.168 (8) Å via a bidentate coordination are consistent with the previously published structure of esomeprazole magnesium water–butanol solvate (Skieneh *et al.*, 2016). Mg—O(H$_2$O) bond lengths of 2.084 (7) Å to $W1$ are also consistent with previously published bond lengths (Skieneh *et al.*, 2016). The two additional molecules of water ($W2$) donate hydrogen bonds to the pyridyl nitrogen atom of each omeprazolate, with O···N distances of 2.833 (13) Å. Each $W1$ water molecule also takes part in hydrogen-bond donation to the benzimidazolate nitrogen atom of an adjacent omeprazolate anion [O···N = 2.745 (10) Å], leading to the formation of layers of molecules in the *bc* plane as shown in Fig. 3. $W1$ also forms two separate hydrogen bonds to $W2$ (O—O distances of 2.692 and 3.018 Å). Thus, the magnesium-bound water $W1$ is tetra-coordinated, while $W2$ is tri-coordinated.

As discussed in Section 2.5, the hydrogen positions on the water molecules were computationally varied to see if a slightly different hydrogen-bond network would generate a more stable structure. The two alternative structures were refined using *CASTEP* under the same symmetry constraints and their DFT-D energies compared. It was found that the structure where the O—H bonds of the Mg-bound $W1$ water are aligned roughly parallel to the O(S)—Mg—O(S) bonds [Fig. 4(*a*)] are about 0.7 kcal mol^{-1} (1 kcal mol^{-1} = 4.184 kJ mol^{-1}) more stable than when they are aligned roughly parallel to the N—Mg—N bonds [Fig. 4(*b*)]. To
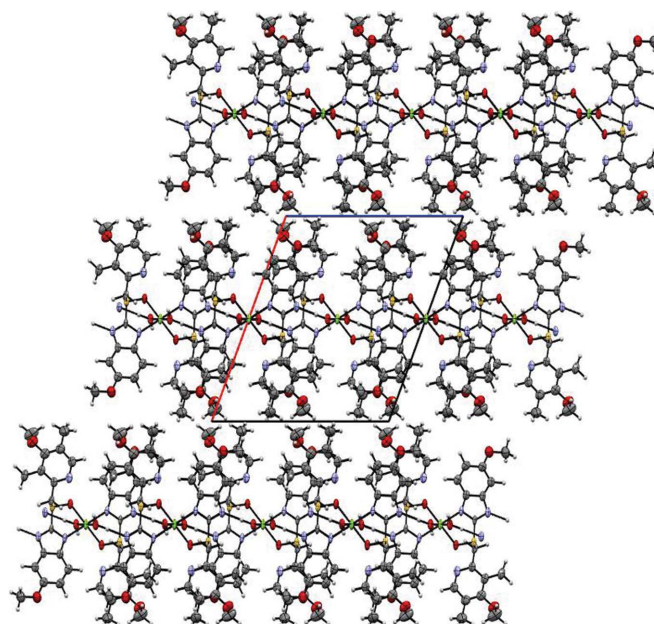

Figure 2
The molecular structure of diaquabis(omeprazolate)magnesium dihydrate (DABOMD). Displacement ellipsoids are shown at the 50% probability level. Intermolecular hydrogen bonds between the molecules in the unit cell are shown as blue dotted lines. Atoms are coloured as follows: Mg green, S yellow, N blue, O red, C grey and H white.
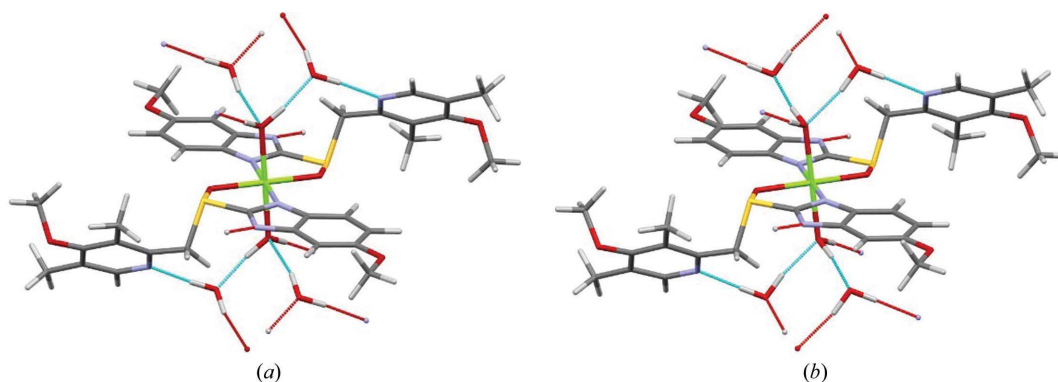

Figure 3
The crystal packing arrangement of DABOMD, viewed down the crystallographic *b* axis. Displacement ellipsoids are shown at the 50% probability level. Additional $W2$ water molecules have been omitted for clarity. Intermolecular hydrogen bonds between the molecules in the unit cell are shown as dotted lines. Atoms are coloured as follows: Mg green, S yellow, N blue, O red, C grey and H white.
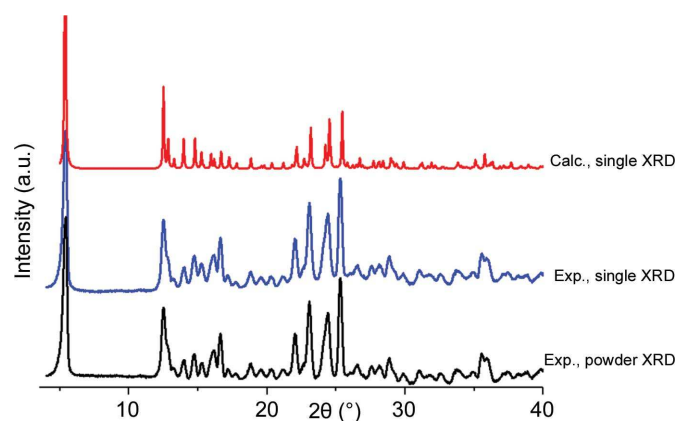
Figure 4
CASTEP optimized DABOMD crystal structures with different hydrogen-bond directions.

quantify the water binding in the preferred *CASTEP* optimized crystal, their intermolecular interactions were calculated using B3LYP-D3/6-31G (d, p) by removing the water molecules pairwise from the crystal structure and making further individual energy calculations on the separated parts. Interestingly, the two pairs of water molecules bind with distinctly separate strengths, -26.8 and -35.5 kcal mol^{-1}, where the $W1$ binding to the magnesium cation are more strongly bound. This result will be discussed further in the TGA section below.

Fig. 5 shows XRPD patterns of DABOMD from simulated data, experimental data from ground single crystals and experimental data from DABOMD powder. The powder and ground single-crystal XRPD patterns look similar and are in close agreement with the simulated pattern from the single crystal. A slight shift in 2θ for the calculated XRPD curve may be due to the difference in temperature, since XRPD was run at room temperature, unlike the single-crystal determination which was performed at 120 K. The difference in temperature is expected to give rise to an expansion in the unit-cell dimensions at room temperature.

To confirm the total water content in the crystal structure, thermogravimetric analysis (TGA) was performed. The TGA results shown in Fig. 6 reveal two different episodes of mass loss for DABOMD crystalline powder. The total amount of mass loss in both events is 8.6%, which indicates two water molecules released at each event. These results are consistent with the single-crystal XRD analysis and the intermolecular interaction analysis, which indicate that the first two water molecules ($W2$) that are hydrogen bonded only are lost at a lower temperature, followed by the water molecules coordinated to the magnesium cation ($W1$).

DSC analysis was performed on DABOMD crystalline powder (Fig. 7). The DSC patterns display three distinct
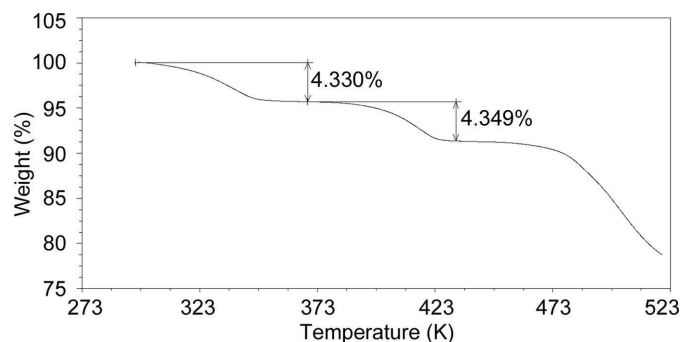
Figure 6
Thermogravimetric analysis plot of DABOMD crystalline powder heated from 298 to 523 K at a rate of 5 K min^{-1}.
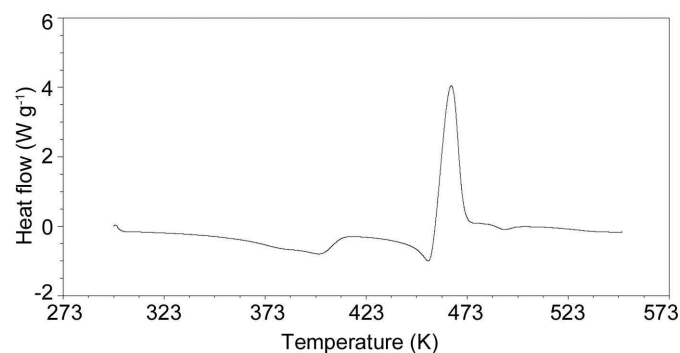

Figure 5
XRD patterns of DABOMD, (top) simulated from single-crystal data, (middle) experimental data from ground single crystals and (bottom) experimental data from bulk powder.

Figure 7
Differential scanning calorimetry plot of DABOMD crystalline powder heated from 298 to 563 K at a rate of 5 K min^{-1}.
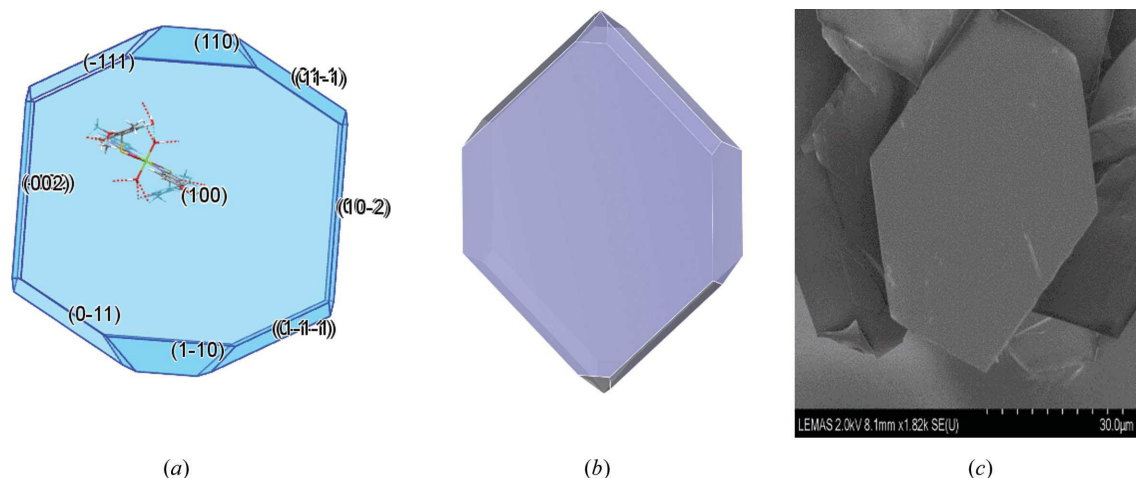
Figure 8
DABOMD. (*a*) Predicted morphology using the BFDH model. (*b*) Predicted morphology using growth morphology. (*c*) Experimental morphology.

thermal events: an endothermic peak at 382 K, followed by another endothermic peak at 446 K and an exothermic peak at 470.95 K. The first endothermic peak corresponds to a water-loss event. A similar observation was reported for the de-hydration of sodium omeprazole (Murakami *et al.*, 2009) and the loss of water from the crystal structure for magnesium esomeprazole water–butanol solvate (Skieneh *et al.*, 2016). The second endothermic event in Fig. 7 corresponds to the loss of the more strongly bound water. The exothermic peak corresponds to a decomposition process of the crystalline form of magnesium omeprazolate (Murakami *et al.*, 2009; Skieneh *et al.*, 2016), as confirmed by hot-stage microscopy visual analysis (not shown).

3.1.1. Crystal habit. The crystal habit may influence downstream pharmaceutical processes, *e.g.* flowability, comminution and compaction. Crystal habit also plays a role in the dissolution rate of drugs, depending on the functional groups exposed on the surface (Storey & Ymen, 2011; Sun & Grant, 2001; Modi *et al.*, 2014). The crystal habit can be obtained experimentally from growing single crystals and can be simulated using *in silico* tools such as BFDH morphology or attachment energy models. During the process of milling, it is assumed that the morphology of the crystal is a major factor in the fracture mechanism which can occur by geometric or thermodynamically driven mechanisms (Halme *et al.*, 2019). The geometric mechanism describes fracture along the shortest dimension of a crystal, for example a typical breakage of a long needle. The thermodynamic mechanism is where the crystals tend to minimize their surface energies to produce a crystal habit where the dominant faces are those exhibiting a lower energy (Shariare *et al.*, 2012). Thus, crystal growth methods based on calculation of E_{att} can produce a more accurate morphology prediction than the BFDH method (Halme *et al.*, 2019; Sun & Kiang, 2008). The habits produced (Fig. 8) show that DABOMD exhibits a hexagonal plate morphology in both the experimentally grown and the modelled crystals, with similar overall shapes.

The Zingg diagram characterization for DABOMD produces the following dimension ratios: intermediate/long =

0.9 and short/intermediate = 0.5, which further support its platelet morphology (Fig. 9). Chikhalia and co-workers stated that crystals exhibiting a plate-like morphology are more prone to disorder during milling compared with those exhi-biting needle morphology (Chikhalia *et al.*, 2006). In general, it was suggested that particles exhibiting a high elongation ratio (longest dimension over shortest dimension) reduce in size more rapidly (Halme *et al.*, 2019; Shariare *et al.*, 2012), for example paracetamol and AZD5423, which have elongation ratios of 2.1 and 3.4, respectively (Halme *et al.*, 2019). For DABOMD, the calculated elongation ratio from BFDH and 2D images is 2.2, which is equivalent to a high elongation ratio according to Halme *et al.* (2019), although the shape alone is not sufficient to predict the particle breakage behaviour (de Vegt, 2007; Shariare *et al.*, 2012; Halme *et al.*, 2019). Moreover, the surfaces produced by the BFDH model show that (100), (102), (011) and (1$\bar{1}$0) are among the major surfaces, with (100) being the most dominant face. The major face produced by the BFDH model coincides with that produced from the growth morphology calculations. Here, (100) occupies more than 59% of the surface area (Table 4) and exhibits an E_{att} value of -25.8 kcal mol^{-1}, followed by the (011) and (11$\bar{1}$) surfaces which possess E_{att} values of -75.9 and -78.8 kcal mol^{-1}, respectively. Roberts and co-workers stated
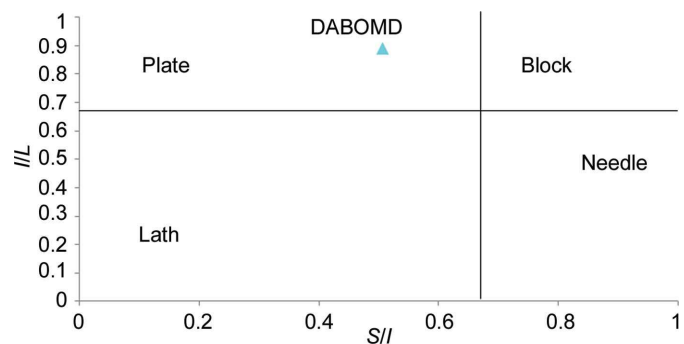
Figure 9
A plot of a Zingg diagram, where *L* is the longest dimension, *I* is the intermediate dimension and *S* is the shortest dimension.

Table 4
DABOMD results from attachment energy (E_{att}) calculations of growth morphology.

| (hkl)	Multiplicity	d_{hkl} (Å)	Total E_{att} (kcal mol^{-1})	Area (%)
(100)	2	16.43	−25.8	59.4
(011)	4	6.89	−75.9	21.5
(11$\bar{1}$)	4	6.80	−78.8	9.0
(110)	4	7.23	−80.9	2.0
(10$\bar{2}$)	2	7.08	−101.7	8.1

that the face with the least negative E_{att} represents the slowest growing face and is the major habit face of the crystal (Roberts *et al.*, 1994). Hence, it can be concluded that face (100) is the major face of DABOMD.

3.2. Slip planes

The fracture or cleavage planes of crystals are important when it comes to milling and tabletting (Storey & Ymen, 2011; Sun & Kiang, 2008). Identification of these crystallographic planes, if any exist, gives valuable mechanistic information when it comes to understanding the behaviour of crystals during processing. Slip or cleavage planes in a crystal are the planes that have the weakest interactions between closest planes. Intuitively, one would expect that the deformation will usually involve crystal planes that are the easiest to displace when the crystal is subjected to stress. Cleavage properties are not only important where particle fracture is more likely to occur or increase the surface area, but also change the relative exposure of different crystal faces and therefore the surface chemistry, which may lead to increased adhesion or cohesion (Storey & Ymen, 2011). Furthermore, ductile breakage is thought to occur through slip planes (Duncan-Hewitt *et al.*, 1994).

Multiple approaches have been used to characterize the slip planes. One such approach involves the use of interplanar spacing, where the slip planes are the planes of highest molecular density (often strengthened by hydrogen bonds between the planes) and largest *d* spacing compared with other planes (Bandyopadhyay & Grant, 2002). A qualitative visualization accompanied by the calculation of E_{att}, where the planes with the lowest E_{att} are thought to be slip planes, was for a long time a commonly accepted technique for the identification of slip planes (Sun & Kiang, 2008). More recently, however, it has been emphasized that more advanced sets of predictive tools such as energy frameworks and DFT calculations should be performed as well, to get a more comprehensive view (Halme *et al.*, 2019; Putra *et al.*, 2016; Wang & Sun, 2018, 2019).

Table 4 shows that the (100) plane has the largest *d* spacing in DABOMD, with d_{hkl} = 16.43 Å, which implies that it could serve as a candidate slip plane. Shariare *et al.* (2012) concluded that, generally, materials with the lowest *d* spacing tend to exhibit a brittle failure, as these planes are more strongly interacting. Hence, *d*-spacing analyses could serve as an initial indicator, even in the absence of single-crystal structure data, given that *d* spacings can be obtained from X-ray powder
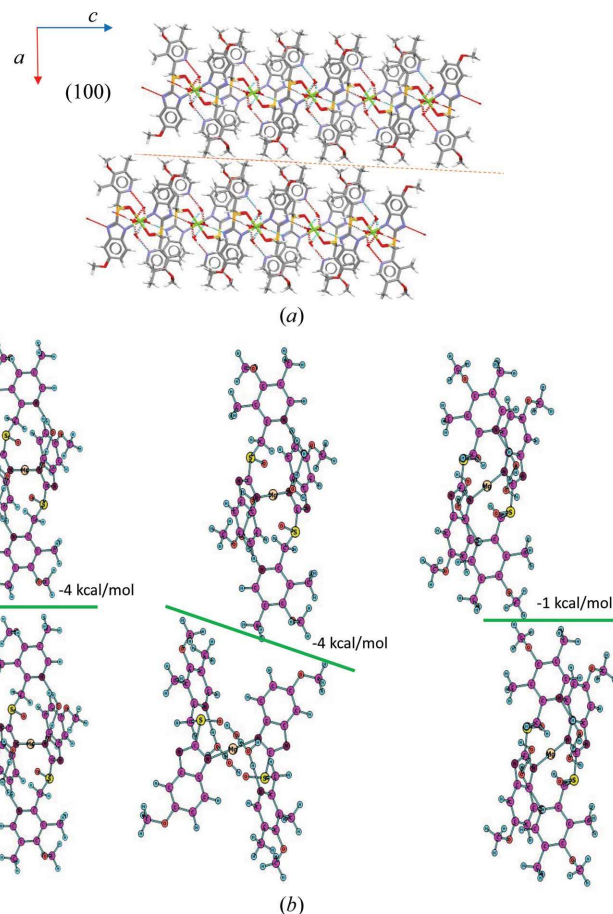
Figure 10
(*a*) Visualization of the potential (100) slip plane in the DABOMD crystal structure. (*b*) Quantifications of interactions along the (100) plane visualized as green lines.

diffraction data (Shariare *et al.*, 2012) and other techniques. However, the *d*-spacing correlation is not expected to work for some materials due to other factors such as the type of hydrogen-bonding framework (Shariare *et al.*, 2012; Halme *et al.*, 2019).

Qualitative visualization of the (100) plane [Fig. 10(*a*)] indicates the presence of a slip plane between the methyl and methoxy groups present in DABOMD, and no strong hydrogen bonding crossing the plane. Thus, the crystal interaction is here controlled by weaker dispersion forces or only weak C—H⋯O bonds. Other potential slip planes [(011) and (11$\bar{1}$)] are controlled by classical hydrogen bonds or ionic interactions, and thus are more strongly interacting and held together.

Quantitative analysis from the attachment energy calculations (Table 4) indicates that the (100) plane can serve as a candidate slip plane since it clearly has the least negative E_{att}. It is thought that surfaces with the least negative E_{att} are the most probable cleavage planes since they are the most weakly bound to the crystal face (Roberts *et al.*, 1994). Sun & Kiang (2008) examined the slip planes of 14 crystals using the E_{att} model and concluded that this model yields only roughly 50% success. The nature of the slip plane can determine the possibility of slip occurring. The prediction of slip planes using

E_{att} can produce inaccurate results for crystals that typically exhibit zigzag or corrugated layers or slip planes (Sun & Kiang, 2008). Also, Shariare *et al.* (2012) and Halme *et al.* (2019) concluded that materials that show ductile behaviour tend to encompass flat slip planes due to the relatively lower force required to induce a displacement in flat slip planes compared with corrugated ones. Moreover, it can be seen in Fig. 10(*a*) that DABOMD has a rather flat candidate slip plane on (100), which further supports the results obtained from the *d* spacing and the E_{att} calculation model.

The presence of flat or corrugated slip planes is also related to the slip directions. Materials exhibiting corrugated slip planes are more likely to glide in two dimensions upon stress, whereas particles exhibiting flat slip planes are more likely to slip in various directions (Halme *et al.*, 2019).

We also computed the interaction energies along the (100) plane using DFT energies via the *CrysIn* tool. The interactions between methyl and methoxy groups result in a weak stabilization of only -1 to -4 kcal mol^{-1}, as visualized in Fig. 10(*b*). Other potential slip planes were also analysed and found to exhibit stronger interactions due to multiple hydrogen bonds.

In summary, the qualitative observation of the BFDH morphology, E_{att} calculations and *CrysIn* analysis all indicate that (100) is a candidate slip plane for magnesium omeprazole

dihydrate. Thus, it can be suggested that DABOMD will experience a plastic deformation across the candidate slip plane (100) and will probably demonstrate a great propensity for breakage and size reduction during milling. Further characterization of the impact of milling behaviour on DABOMD is underway and will be communicated in due course.

3.3. Mechanical properties

Successful comminution of API powders requires an understanding of the particle mechanical properties, since they dictate how the material would behave upon milling. The elastic properties of drug pharmaceuticals can determine many aspects of their subsequent processing properties, since they are largely related to the forces between the molecules. Experimentally, the elastic properties of single crystals are difficult to measure due to the difficulties of growing a single crystal of an adequate size. Based on the crystal structure of the API, the elastic constant or the Young's modulus of elasticity is obtained from the calculation of intermolecular interactions in the form of force constants that characterize both normal and shear stress (Beyer *et al.*, 2001).

The results presented in Table 5 show that DABOMD possesses various Young's moduli across the *x*, *y* and *z* directions. Overall, the crystal system is rather isotropic

Young's modulus

| Young's modulus in (*xy*) plane | Young's modulus in (*xz*) plane | Young's modulus in (*yz*) plane |
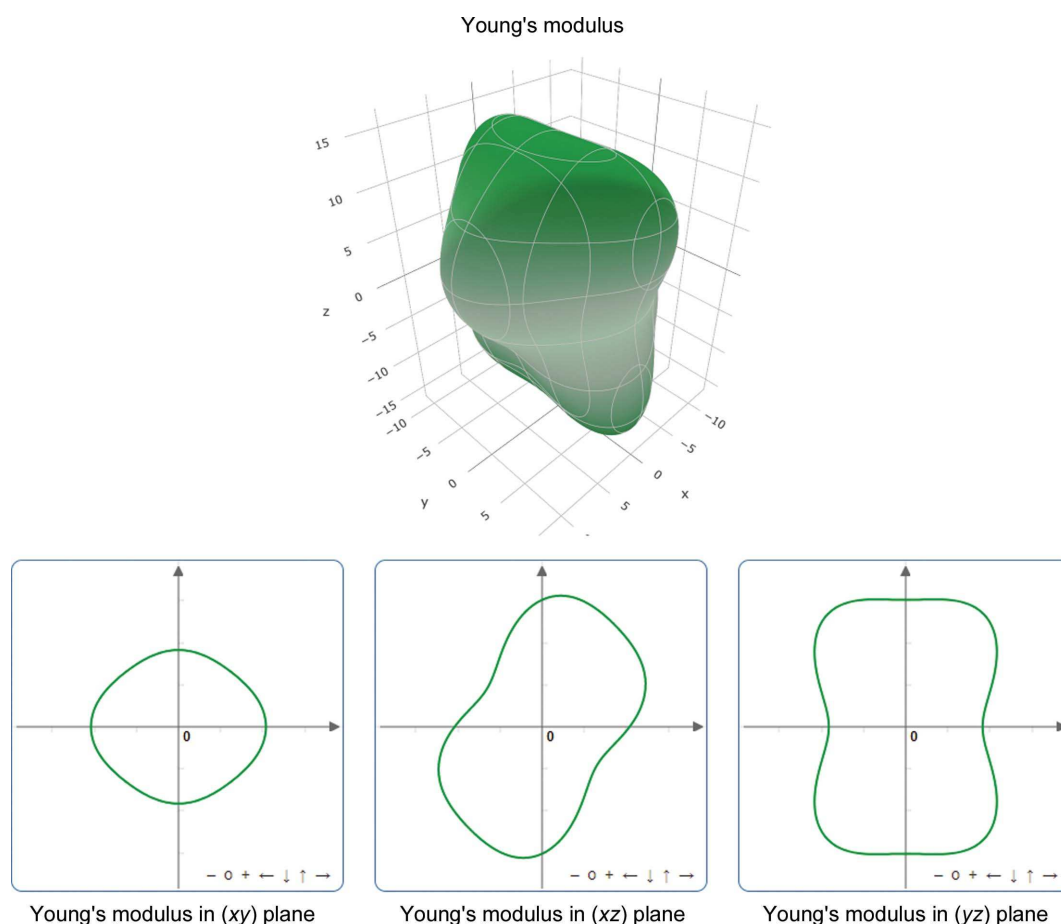
Figure 11
The anisotropy of the elastic moduli of DABOMD in different directions and planes. The highest Young's modulus is found along the *z* axis.

Table 5
*CASTEP* computed values of Young's modulus along different crystal axes for DABOMD.

Axis	Young's modulus (GPa)
x	10.38
y	9.12
z	15.09
Minimum	7.94
Maximum	16.45

(anisotropy value of 2.1; see Fig. 11), but the Young's moduli in different directions are on the borderline of classifying the material as soft to moderately hard according to the classification suggested by Rowe & Roberts (1995). DABOMD has its lowest Young's modulus in the x (10.38 GPa) and y directions (9.12 GPa), so according to the classification it could potentially behave like a soft material with a tendency to plastic deformations, if the crystal were stressed across the x or y direction (Fig. 12). It exhibits its highest Young's modulus in the z direction (15.1 GPa), which classifies the crystal under a different category during stressing events. It should be pointed out that the z direction is linked to the crystallographic dimension where the most hydrogen bonds are located (Fig. 12), thus making this a more strongly bound crystalline direction, while the x direction is perpendicular to the (100) slip plane (Figs. 10 and 12).

4. Conclusions

We have reported the single-crystal structure of diaquabis(omeprazolate)magnesium dihydrate (DABOMD), which encompasses four water molecules, two of which are directly coordinated to the magnesium cation while the other two are hydrogen bonded to the pyridine functionality. DFT calculations show that the water molecules coordinated to magnesium are more strongly bonded in the crystal structure than the hydrogen-bonded water molecules. The expected difference in water mobility is qualitatively verified in TGA experiments, where two separate mass losses are observed at different temperatures. The qualitative and quantitative analysis of the crystal growth morphology shows that DABOMD displays as a hexagonal plate, has a slip plane through the (100) face and exhibits a slightly anisotropic Young's modulus. These results suggest that DABOMD is likely to experience great disorder and plastic deformation during the process of milling.

While single-crystal X-ray diffraction provides information on molecular structure, the use of computational modelling tools provides a better understanding of the underlying structure of a crystal, including the inter- and intramolecular interactions. For example, the correlation between single-crystal XRD and crystal interaction calculation tools in this work provides valuable information on the nature of the bonds and intermolecular interactions present in the crystal structure. Understanding the nature and the strength of these bonds is a valuable application of crystal engineering of organic and organometallic crystals.
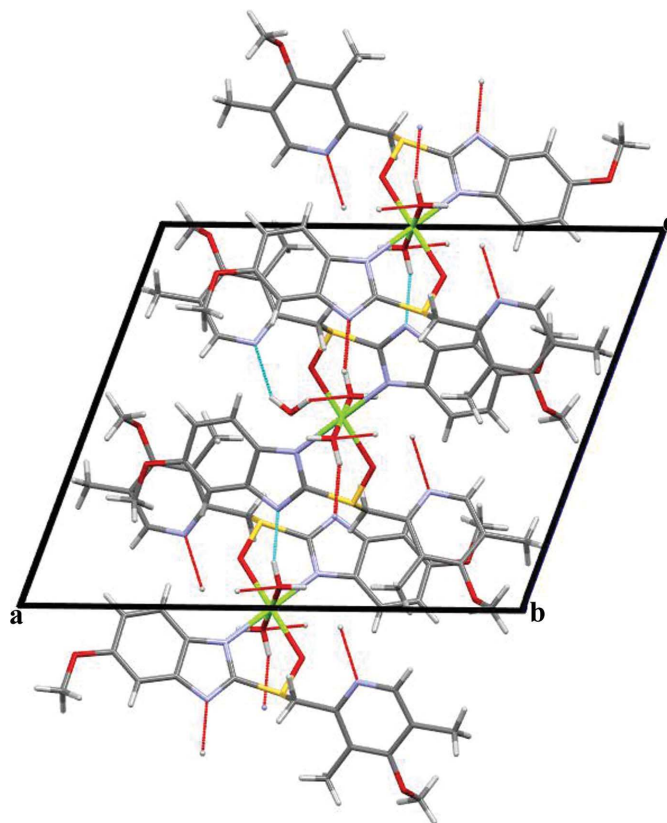
Figure 12
The hydrogen bonding in the DABOMD crystal structure, mainly along the z direction, visualized by red and turquoise dashed lines.

This investigation shows that the use of crystal geometry and d spacing may serve as a preliminary tool for predicting the fracture propensity of a material. The use of computational approaches such as the attachment energy model and intermolecular pair interactions give more precise and consistent results about the slip plane in which a fracture or ductile failure is likely to occur and it is recommended that they are used. For this system, these computational approaches are in agreement with the qualitative visualization of the slip plane which sometimes gives less accurate results. Furthermore, the calculation of elastic moduli allows for the quantification of the intermolecular forces in three dimensions and makes a good complementary tool for the calculation of attachment energy and intermolecular pair interactions.

The techniques used in this paper have proved to be consistent and successful and can provide a thorough prediction of the mechanistic behaviour of DABOMD. The combination of methods can be used as fast screening tool for fine-powder pharmaceuticals for which the mechanical properties are difficult and time-consuming to measure experimentally.

research papers

References

Bandyopadhyay, R. & Grant, D. J. W. (2002). *Pharm. Res.* **19**, 491–496.

Beyer, T., Day, G. M. & Price, S. L. (2001). *J. Am. Chem. Soc.* **123**, 5086–5094.

Bhatt, P. M. & Desiraju, G. R. (2007). *Chem. Commun.* pp. 2057–2059.

Chikhalia, V., Forbes, R. T., Storey, R. A. & Ticehurst, M. (2006). *Eur. J. Pharm. Sci.* **27**, 19–26.

Clark, S. J., Segall, M. D., Pickard, C. J. II, Hasnip, P. J., Probert, M. I. J., Refson, K. & Payne, M. C. (2005). *Z. Kristallogr.* **220**, 567–570.

Day, G. M., Price, S. L. & Leslie, M. (2001). *Cryst. Growth Des.* **1**, 13–27.

Docherty, R., Roberts, K. J. & Dowty, E. (1988). *Comput. Phys. Commun.* **51**, 423–430.

Duncan-Hewitt, W. C., Mount, D. L. & Yu, A. (1994). *Pharm. Res.* **11**, 616–623.

Frisch, M. J. *et al.* (2016). *GAUSSIAN16*. Gaussian Inc., Wallingford, Connecticut, USA.

Gaillac, R. (2016). *J. Phys. Condens. Matter*, **28**, 275201.

Gavezzotti, A. (2005). *Z. Kristallogr. Cryst. Mater.* **220**, 499–510.

Gustavsson, A. & Kjellbom, K. Y. I. (1997). *Omeprazole Sodium Salt*. US Patent 6207188 B1

Halme, A., Quayle, M. J., Nilsson Lill, S. O., Pettersen, A., Fransson, M. & Boissier, C. (2019). *Cryst. Growth Des.* **19**, 3670–3680.

Hultman, I., Stenhoff, H. & Liljeblad, M. (2007). *J. Chromatogr. B*, **848**, 317–322.

Macrae, C. F., Bruno, I. J., Chisholm, J. A., Edgington, P. R., McCabe, P., Pidcock, E., Rodriguez-Monge, L., Taylor, R., van de Streek, J. & Wood, P. A. (2008). *J. Appl. Cryst.* **41**, 466–470.

Mishra, M. K., Ramamurty, U. & Desiraju, G. R. (2015). *J. Am. Chem. Soc.* **137**, 1794–1797.

Modi, S. R., Dantuluri, A. K. R., Perumalla, S. R., Sun, C. C. & Bansal, A. K. (2014). *Cryst. Growth Des.* **14**, 5283–5292.

Murakami, F. S., Lang, K. L., Mendes, C., Cruz, A. P., Carvalho Filho, M. A. & Silva, M. A. S. (2009). *J. Pharm. Biomed. Anal.* **49**, 72–80.

Ohishi, H. (1990). *ChemInform*, **21**, 1921–1923.

Payne, R. (1996). *Int. J. Pharm.* **145**, 165–173.

Perdew, J. P., Burke, K. & Ernzerhof, M. (1996). *Phys. Rev. Lett.* **77**, 3865–3868.

Putra, O. D., Yoshida, T., Umeda, D., Higashi, K., Uekusa, H. & Yonemochi, E. (2016). *Cryst. Growth Des.* **16**, 5223–5229.

Roberts, R. J., Rowe, R. C. & York, P. (1994). *J. Mater. Sci.* **29**, 2289–2296.

Rowe, R. C. & Roberts, R. J. (1995). *Adv. Pharm. Sci.* **7**, 1–62.

Shariare, M. H., Leusen, F. J., de Matas, M., York, P. & Anwar, J. (2012). *Pharm. Res.* **29**, 319–331.

Sheldrick, G. M. (2015a). *Acta Cryst.* C**71**, 3–8.

Sheldrick, G. M. (2015b). *Acta Cryst.* A**71**, 3–8.

Skieneh, J., Khalili Najafabadi, B., Horne, S. & Rohani, S. (2016). *Molecules*, **21**, 544.

Storey, R. A. & Ymen, I. (2011). *Solid-state Characterization of Pharmaceuticals*. Chichester: John Wiley & Sons.

Sun, C. & Grant, D. J. W. (2001). *J. Pharm. Sci.* **90**, 569–579.

Sun, C. C. & Kiang, Y. H. (2008). *J. Pharm. Sci.* **97**, 3456–3461.

Toplak Casar, R. L. (2013). *Process for the Preparation of Esomeprazole Magnesium Dihydrate*. US Patent 8362259 B2.

Turner, M. J., Thomas, S. P., Shi, M. W., Jayatilaka, D. & Spackman, M. A. (2015). *Chem. Commun.* **51**, 3735–3738.

Vegt, O. M. de (2007). PhD thesis, Rijksuniversiteit Groningen, Groningen, The Netherlands.

Wang, C. & Sun, C. C. (2018). *Cryst. Growth Des.* **18**, 1909–1916.

Wang, C. & Sun, C. C. (2019). *Mol. Pharm.* **16**, 1732–1741.